Photoelectron Spectroscopy and Thermochemistry of the Peroxyformate Anion

Stephanie M. Villano, Nicole Eyet,† Scott W. Wren, G. Barney Ellison, Veronica M. Bierbaum,* and W. Carl Lineberger*

JILA, University of Colorado and the National Institute of Standards and Technology and Department of Chemistry and Biochemistry, University of Colorado, Boulder, Colorado 80309-0440

Received: August 5, 2009; Revised Manuscript Received: September 28, 2009

The 351.1 nm photoelectron spectrum of the peroxyformate anion has been measured. The photoelectron spectrum displays vibronic features in both the $\tilde{X}^2A''$ ground and $\tilde{A}^2A'$ first excited states of the corresponding radical. Franck−Condon simulations of the spectrum show that the ion is formed exclusively in the trans-conformation. The electron affinity (EA) of the peroxyformyl radical was determined to be 2.493 ± 0.006 eV, while the term energy splitting was found to be $0.783^{+0.060}_{-0.020}$ eV. Extended progressions in the C−OO (973 ± 20 cm^{-1}) and O−O (1098 ± 20 cm^{-1}) stretching modes are observed in the ground state of the radical. The fundamental frequency of the in-plane OCO bend was found to be 574 ± 35 cm^{-1}. The gas-phase acidity of peroxyformic acid has been determined using an ion−molecule bracketing technique. On the basis of the size of the trans- to cis- isomerization barrier, the measured acidity was assigned to the higher energy trans-conformer of the acid. The gas-phase acidity of the lower energy cis-conformer of peroxyformic acid was found from the measured acidity for the trans-form and a calculated energy correction: $\Delta_a G_{298}$(*cis*-peroxyformic acid) = 346.8 ± 3.3 kcal mol^{-1} and $\Delta_a H_{298}$(*cis*-peroxyformic acid) = 354.4 ± 3.3 kcal mol^{-1}. Using a negative ion EA/acidity thermochemical cycle, the O−H bond dissociation energy (D_0) values of the trans- and cis-conformers of peroxyformic acid to form the trans-radical were determined to be 94.0 ± 3.3 and 97.1 ± 3.3 kcal mol^{-1}, respectively. The heat of formation ($\Delta_f H_{298}$) of the *trans*-peroxyformyl radical was found to be −22.8 ± 3.5 kcal mol^{-1}.

Introduction

The reaction of formyl radical with molecular oxygen has received considerable attention, due to its prominent role in tropospheric and hydrocarbon combustion processes.

$$HCO + O_2 \rightarrow HO_2 + CO \qquad (1)$$

A variety of techniques have been employed to determine the room temperature reaction rate,[1–13] and the formation of HO_2 has been observed using laser magnetic resonance spectroscopy.[14] While there has been some controversy on the exact temperature dependence[6,9,10,13] as well as the effect of isotopic substitution,[7,13] the consensus is that this reaction proceeds via an activated peroxyformyl collision complex, [HC(O)OO]*.[7,15–20] Hsu et al.[15] have investigated the various product channels using ab initio molecular orbital and statistical calculations. These results indicate that the vibrationally excited peroxyformyl complex rapidly dissociates via a four-membered cyclic transition state structure to form HO_2 + CO. Direct formation of these products via hydrogen abstraction was found to be negligible at temperatures below 2000 K. At pressures below 2000 Torr, deactivation of the peroxyformyl radical by a third body collision was also found to be insignificant. The results of this study are consistent with previous experimental observations, which found that the rate constant is pressure-independent over the range of 5−1000 Torr.[2,7,8]

To date, the only experimental observation of the peroxyformyl radical has been via matrix isolation IR-spectroscopy. In this technique, transient reaction intermediates, which readily dissociate in the gas phase, are stabilized through multiple collisions when trapped in the matrix environment. In an early study, this radical was produced by the photolysis of formaldehyde in a solid oxygen matrix.[17,18] The assignment of the spectral features, however, was complicated by the presence of the HO_2 radical, which was likely present in the photolysis cage. More recently, the peroxyformyl radical has been studied by discharge production and deposition of the formyl radical onto a solid argon matrix followed by an association reaction with oxygen.[19] Two vibrational transitions at 1821.5 and 957.3 cm^{-1} have been assigned to the C=O and C−OO stretching modes, respectively. The spectral assignments were confirmed by ^{18}O isotopic labeling and by electronic structure calculations.

In this work, we report the first observation of the isolated peroxyformyl radical. This has been achieved through electron photodetachment from the peroxyformyl anion. Analysis of the photoelectron energy spectrum allows determinations of the electron affinity, term energy splitting, and vibrational frequencies of the peroxyformyl radical and provides insight into the molecular structure of both the anion and radical species. Additionally, the gas-phase acidity of peroxyformic acid was determined from ion−molecule bracketing experiments. Combining this gas-phase acidity with the peroxyformyl radical electron affinity in a negative ion thermochemical cycle[21–24] allows the determination of the O−H bond dissociation energy in peroxyformic acid. Electronic structure calculations provide additional insight into the structural and energetic aspects of the peroxy ion, the radical, and the parent acid. This paper

* Corresponding authors. E-mail: veronica.bierbaum@colorado.edu (V.M.B.); wcl@jila.colorado.edu (W.C.L.).

† Current address: Department of Chemistry, Saint Anselm College, 100 Saint Anselm Dr. #1760, Manchester, New Hampshire 03102.

10.1021/jp907569w
Published on Web 10/14/2009

represents a continuation of our studies on the thermochemistry, spectroscopy, and reactivity of peroxy compounds.[25–32]

Experimental Details

Negative Ion Photoelectron Spectroscopy. A detailed description of the anion photoelectron spectrometer that was used in these studies has been provided elsewhere.[28,33,34] The peroxyformate anion [$HC(O)OO^-$] was synthesized in a flowing afterglow source through the following series of ion−molecule reactions that occur sequentially downstream from a microwave discharge source forming O^- anions.

$$O^- + CH_4 \rightarrow CH_3 + OH^- \quad (2)$$

$$OH^- + H_2O_2 \rightarrow H_2O + HOO^- \quad (3)$$

$$HOO^- + HC(O)OR \rightarrow HC(O)OO^- + ROH \quad (4)$$

The final step is a gas-phase Baeyer−Villiger reaction, previously studied by DePuy and co-workers,[35,36] in which methyl formate [$HC(O)OCH_3$] or ethyl formate [$HC(O)OCH_2CH_3$] reacts with HOO^-. The large number of collisions in the source region (~0.5 Torr, 3−10 ms residence time) ensures that the ions are thermalized to ~298 K. Negative ions are gently extracted from the source region and passed through a Wien velocity filter for mass selection. The mass selected ion beam is then crossed with a 351.1 nm (3.531 eV) line from a cw argon ion laser in an external build-up cavity producing ~100 W of circulating power. Photoelectrons that are ejected into a small ($4\pi/2000$) solid angle perpendicular to the plane formed by the photon and ion beams are analyzed by a hemispherical kinetic energy analyzer coupled to a position sensitive detector. The photoelectron spectrum is a plot of electron kinetic energy (eKE) versus photoelectron counts. The energy scale is converted to electron binding energy (eBE) by subtracting the electron kinetic energy from the photon energy.

The energy resolution ranges from 8 to 15 meV fwhm. The absolute energy scale is calibrated with the well-known electron affinity (EA) of the sulfur atom[37] and a small energy scale compression factor (<1%), which is derived from the photoelectron spectra of reference ions S^-, I^-, and O^- using the EAs of the corresponding atoms.[33,37] Angular distribution measurements at a given electron kinetic energy (KE) were conducted by changing the angle (θ) between the electric field vector of the laser beam and the photoelectron collection axis. The anisotropy parameter (β), which characterizes the angular distribution of the photoelectrons, is given by the expression[38]

$$\frac{d\sigma}{d\Omega} = \frac{\sigma_{tot}}{4\pi}[1 + \beta(KE)P_2(\cos\theta)] \quad (5)$$

where

$$P_2(\cos\theta) = \frac{3\cos^2\theta - 1}{2} \quad \text{and} \quad -1 \le \beta \le 2 \quad (6)$$

In practice, we obtain the anisotropy parameter from measurements at two collection angles,

$$\beta(KE) = \frac{I_{0°} - I_{90°}}{1/2I_{0°} + I_{90°}} \quad (7)$$

where $I_{0°}$ and $I_{90°}$ are the photoelectron counts at $\theta = 0°$ and $\theta = 90°$, respectively. In addition, spectra are collected at the magic angle ($\theta = 54.7°$), where the photoelectron intensity I(KE) is free from angular dependence.

While the electron energy resolution in these experiments is ~12 meV, the electron binding energy corresponding to an isolated transition can easily be determined to an accuracy of ±5 meV (0.12 kcal mol^{-1}). If that peak is associated with the transition from the ground state of the anion to the ground state of the neutral, the corresponding electron affinity can be determined with similar accuracy. The presence of unresolved structure reduces the accuracy of the experimental result, but the Franck−Condon modeling of the full spectrum still allows quantitative assessments of the experimental error in the binding energy measurements.

Flowing Afterglow-Selected Ion Flow Tube (FA-SIFT) Measurements. The gas-phase acidity (Δ_aG_{298}) of peroxyformic acid was determined from an ion−molecule bracketing technique[39] using a tandem flowing afterglow-selected ion flow tube instrument, which has been described in detail elsewhere.[40] In this method, the peroxyformate anion is allowed to react with several reference acids (AH) of known acidity. If rapid proton transfer is observed, then the reference compound is a stronger acid than peroxyformic acid [$\Delta_aG_{298}(AH) < \Delta_aG_{298}(HC(O)OOH)$]. If proton transfer is not observed, then the reference compound is a weaker acid than the peroxyformic acid [$\Delta_aG_{298}(AH) > \Delta_aG_{298}(HC(O)OOH)$]. By examining the occurrence or nonoccurrence of proton transfer with a series of reference acids, an upper and lower bound can be placed on the acidity of the peroxy acid. As a point of clarification, the gas-phase acidity is the Gibbs free-energy change for heterolytic bond cleavage, $AH \rightarrow A^- + H^+$. Less energy is required to remove a proton from a stronger acid than from a weaker acid; thus, stronger acids have smaller free energy changes than do weaker acids. The enthalpy of deprotonation (Δ_aH_{298}) can be found from eq 8, where Δ_aS_{298}, the entropy of deprotonation, is determined from electronic structure calculations.

$$\Delta_aH_{298}(HC(O)OOH) = \Delta_aG_{298}(HC(O)OOH) + T\Delta_aS_{298}(HC(O)OOH) \quad (8)$$

Peroxyformate anions were formed in a flowing afterglow source using the same synthesis scheme as in the above photodetachment experiments. Negative ions were extracted from the source region and focused into a quadrupole mass filter, which transmits ions with one specific mass-to-charge ratio. The mass selected ion beam was injected into a reaction flow tube whereby the ions are thermalized to a ~298 K rotational and vibrational Maxwell−Boltzmann distribution by collisions with He buffer gas (~0.5 Torr, 10 ms residence time). A measured flow of the neutral reference acid was introduced into the reaction flow tube at various distances through a manifold of inlets. The intensities of the reactant and product ions were measured using a triple quadrupole mass filter coupled to an electron multiplier as a function of reaction time. Neutral reactant flow rates were measured by monitoring the pressure change versus time in a calibrated volume system.

An experimental complication is that, despite injecting the peroxyformate anions with minimal energy, fragment ions [OH^-, HOO^-, and $HC(O)O^-$] formed as a result of collision-induced

dissociation are also present in the reaction flow tube. Since the basicity of some of these fragment ions is greater than that of the parent anion, the deprotonated reference acid was observed even when it is less acidic than peroxyformic acid. Additionally, depletion of the parent peroxyformate anion was also generally observed, since it reacts by neutral O atom loss. In order to determine whether proton transfer occurs between the peroxyformate anion and the reference acid, the intensities of all ions were monitored as a function of time and the contribution from the fragment ions to the deprotonated reference acid signal was removed.

Electronic Structure Calculations. Two different theoretical models, both provided in the Gaussian 03 suite of programs,[41] were used to evaluate structural and energetic aspects of the peroxyformate anion as well as the corresponding protonated and radical species. DFT calculations [B3LYP/6-311++G(d,p)][42–44] were used to calculate optimized geometries, harmonic vibrational frequencies (unscaled), and the rotational constants. The G3MP2B3 composite technique[45] was used to investigate various thermodynamic properties of these species. In this technique, geometries and zero point energies are calculated at the B3LYP/6-31G(d) level of theory followed by a series of well-defined ab initio single-point energy calculations. This method has been tested on a variety of hydrocarbons, and the average deviation from experiment was reported to be 1.25 kcal mol^{-1}.[45] The accuracy of this method was independently evaluated in this work with a test set of molecules that were chosen on the basis of their similarity to the peroxy compound studied here [HOO^-, CH_3OO^-, $C_2H_5OO^-$, $HC(O)O^-$, and $CH_3C(O)O^-$, as well as the corresponding protonated and radical species]. The average deviation from experiment for a set of calculated electron affinities, gas-phase acidities, and bond dissociation enthalpies was found to be 1.5 kcal mol^{-1}.[46] Simulated photoelectron spectra were obtained by calculating the Franck−Condon (FC) factors at a vibrational temperature of 298 K with the PESCAL program.[47] These simulations are based on the B3LYP/6-311++G(d,p)-optimized geometries and normal modes for the anion and corresponding radical species, while electron binding energies are determined from the G3MP2B3 calculations.

Results and Discussion

Photoelectron Spectra of the Peroxyformate Ion. The 351.1 nm magic angle photoelectron spectrum of the *m/z* 61 ion produced from the reaction of HOO^- with ethyl formate is shown in Figure 1a. The same spectral profile is observed when the *m/z* 61 ion is produced from the reaction of HOO^- with methyl formate. The ion−molecule reactivity studies of DePuy and co-workers[35,36] indicate that these reactions proceed via a Baeyer−Villiger reaction to produce the peroxyformate anion rather than the bicarbonate anion, which is the more stable isomer. While our results do not eliminate the possible formation of the latter species, the spectrum in Figure 1a must arise *only* from the peroxyformate anion. The basis for this assertion is that the electron affinity of the bicarbonate radical is ~3.9 eV,[48] and hence, photodetachment of the bicarbonate anion is not energetically possible with the ~3.5 eV photon energy employed in this investigation. The photoelectron angular distribution was measured and the anisotropy parameter (β) is negative across the entire spectrum, consistent with photodetachment from a π-type orbital.[26,28] The most striking feature of the spectrum is the series of intense peaks (b, e, g, h, i, j, k, and m), which are spaced by roughly 1000 cm^{-1}. With the exception of peak b, the width of these peaks is ~50 meV (fwhm), substantially

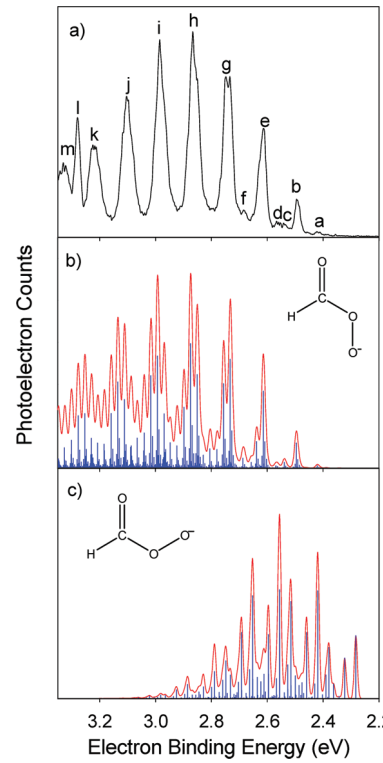

Figure 1. (a) The 351.1 nm magic-angle photoelectron spectrum of the peroxyformate anion collected with ~13 meV resolution. Franck−Condon simulations are shown for transitions from (b) the $\tilde{X}^1A'$ state of the *trans*-peroxyformate anion to the $\tilde{X}^2A''$ state of the *trans*-peroxyformyl radical and (c) the $\tilde{X}A'$ state of the *cis*-peroxyformate anion to the $\tilde{X}^2A''$ state of the *cis*-peroxyformyl radical. The simulations are based on B3LYP/6-311++G(d,p)-optimized geometries and harmonic frequencies; the position of the origin is determined using G3MP2B3 theory. The sticks are the individual Franck−Condon factors, and the solid line is a 13 meV fwhm Gaussian convolution.

greater than the instrument resolution (12−14 meV), indicating that each of these peaks is a composite of multiple vibronic transitions. To confirm this statement, the same spectrum was collected with slightly higher resolution (~8 meV) but lower signal-to-noise ratio; the lower binding energy portion of this higher resolution spectrum is shown in Figure 2a. At this resolution, it is evident that at least peaks e, g, and h have multiple components. Attempts were made to cool the anion beam by surrounding the source flow tube with a liquid nitrogen jacket, which can yield ions with a temperature of ~200 K, resulting in a cleaner, more resolved spectrum. Unfortunately, these attempts were unsuccessful, resulting in the complete loss of ion signal.

There are two stable conformers for the peroxyformate anion. Using G3MP2B3 calculations we have found minima with C_s symmetry that correspond to both the cis- and trans-conformers; these results are summarized in Table 1. At this level of theory, the cis-isomer is predicted to be 5.1 kcal mol^{-1} higher in energy than the trans-isomer. Given this energy difference, the thermal population of the cis-conformer is expected to be negligibly small; however, as shown in Figure 3 (bottom curve), the isomerization barrier that connects the two isomers is sufficiently large (18.3 kcal mol^{-1}) such that the formation of the trans-isomer might be kinetically hindered. The magnitude of this barrier reflects the charge reorganization that occurs as the OCOO dihedral angle is rotated, where in both the trans- and cis-conformations the negative charge is delocalized across the OCOO backbone. In contrast, rotation of the OCOO dihedral

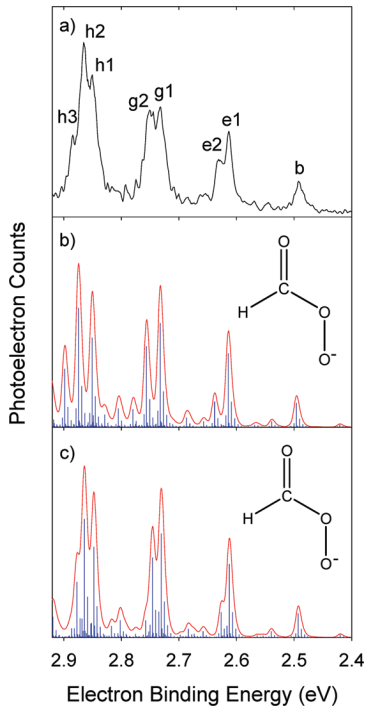

Figure 2. (a) The 351.1 nm magic-angle photoelectron spectrum of the peroxyformate anion collected with ~9 meV resolution. (b) *trans*-Peroxyformate anion Franck−Condon simulation reproduced from Figure 1b. (c) *trans*-Peroxyformate anion Franck−Condon simulation based on B3LYP/6-311++G(d,p)-optimized geometries and harmonic frequencies, but with ν_4, ν_5, and ν_6 in the radical modified to match experimental frequencies. The calculated EA was slightly shifted (<10 meV) to match the experiment.

TABLE 1: Relative Energies (kcal mol^{-1}) of the trans- and cis-Conformers (going from the trans- to the cis-structure) Calculated at the G3MP2B3 Level of Theory[a]

	Δ_0E	$\Delta_{298}H$	$\Delta_{298}G$	$E^{\ddagger}$ $(E + E_{zpt})$
peroxyformic acid	−3.1	−3.4	−2.8	9.5
peroxyformate anion ($\tilde{X}^2A'$)	5.1	5.0	5.1	18.3
peroxyformyl radical ($\tilde{X}^2A''$)	2.4	2.3	2.3	8.4

[a] Δ_0E, $\Delta_{298}H$, and $\Delta_{298}G$ have an estimated uncertainty of ±0.5 kcal mol^{-1}.

angle out of the plane of symmetry localizes the negative charge on the terminal oxygen atom, destabilizing the anion. Due to this large barrier, it may be possible for the peroxyformate anion to be formed with a nonthermal population of isomers. As a side note, along the anion isomerization path there exists a shallow well (<1 kcal mol^{-1}), which corresponds to a quasistable dioxirane intermediate. Under our experimental conditions, this species is not expected to be stable. The conclusion is that calculations do not provide a reliable guide as to whether one or both conformers might be formed under our experimental conditions.

In order to identify which conformer(s) contribute to the observed spectrum, Franck−Condon simulations were performed using the DFT-optimized geometries (Table 2) and harmonic frequencies (Table 3) for the $\tilde{X}^1A'$ state of the peroxyformate anion and the $\tilde{X}^2A''$ state of the peroxyformyl radical for both the trans- and cis-conformations. The location of the electronic band origin is determined using G3MP2B3 calculations. These results are quite distinct from one another, as shown in Figure 1, parts b and c, respectively, where blue sticks correspond to the individual vibronic transitions and the red trace results from convoluting those individual transitions

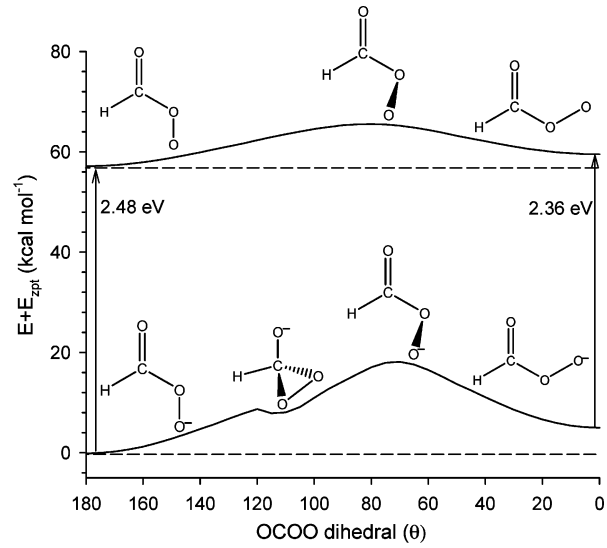

Figure 3. Potential energy surface ($E + E_{zpt}$) calculated at the G3MP2B3 level of theory for the trans- to cis-isomerization of the peroxyformate anion (bottom) and the peroxyformyl radical (top).

with a 13 meV fwhm Gaussian function, which represents the instrument resolution.

The simulated Franck−Condon spectrum (i.e., the width of the profile as well as the relative intensities of the peaks within the profile) for the cis-form of the anion (Figure 1c) is not consistent with the observed spectrum. Additionally, photodetachment is not observed near the calculated EA of 2.36 eV for the *cis*-peroxyformyl radical. These discrepancies indicate that the cis-conformer of the anion is not formed in any appreciable amount. The simulation for the trans-form of the anion (Figure 1b), however, does resemble the observed spectrum. For instance, the simulation is composed of a series of clustered transitions, which correspond to the positions and intensities of the broad series of peaks (b, e, g, h, i, j, k, and m). While the simulation predicts that there are more resolvable transitions than are actually observed, it does capture the essence of the spectral features, including the splitting and relative intensities of the partially resolved peaks collected at higher resolution (Figure 2b). Thus, the observed photoelectron spectrum is *exclusively* attributed to photodetachment of the trans-form of the peroxyformate anion.

Removal of an electron from the out-of-plane π-type orbital on the terminal peroxy oxygen atom of the anion results in the formation of the $\tilde{X}^2A''$ state of the radical. Examination of the DFT-optimized geometries (Table 2) shows significant geometry differences between the trans-anion and the corresponding radical. The most dramatic change is seen in the lengthening of the C−OO bond and tightening of the O−O bond, consistent with the delocalization of the negative charge in the anion across the OCOO backbone. Thus, it is expected that vibrational modes that contain significant distortion along these coordinates will be activated upon photodetachment.

Using the Franck−Condon simulation as a guide, the vibronic features of the ground state of the *trans*-peroxyformyl radical are assigned. Peak b at 2.493 ± 0.006 eV is the electronic band origin, which corresponds to the EA of the peroxyformyl radical. This assignment is in excellent agreement with the G3MP2B3-calculated value of 2.48 eV. The partially resolved peaks e1 and e2 are due to the fundamentals of the in-plane C−OO stretch (ν_5) and the O−O stretch (ν_4), respectively. The first and second overtones of ν_5 appear in the spectrum as peaks g1 and h1. Peaks g2 and h2 are due to one and two quanta of ν_5 on the ν_4

TABLE 2: B3LYP/6-311++G(d,p) Optimized Geometries for Peroxyformic Acid, Peroxyformate Anion, and Peroxyformyl Radical[a]

	peroxyformic acid ($\tilde{X}^1A'$)		peroxyformate anion ($\tilde{X}^1A'$)		peroxyformyl radical ($\tilde{X}^2A''$)		peroxyformyl radical ($\tilde{A}^2A'$)	
	cis	*trans*	*cis*	*trans*	*cis*	*trans*	*cis*	*trans*
C−H	1.096	1.099	1.119	1.105	1.097	1.099	1.096	1.095
C═O	1.202	1.190	1.222	1.227	1.178	1.179	1.185	1.184
C−O	1.341	1.368	1.308	1.304	1.422	1.427	1.387	1.397
O−O	1.441	1.455	1.455	1.480	1.326	1.328	1.365	1.369
O−H	0.982	0.969	–	–	–	–	–	–
∠H−C═O	127.3	127.9	122.1	124.0	129.2	130.4	129.0	128.1
∠H−C−O	108.2	112.1	106.6	111.6	105.5	109.7	104.8	112.1
∠O═C−O	124.4	120.1	131.3	124.4	125.3	119.9	125.3	119.8
∠C−O−O	111.8	108.8	117.7	112.5	114.1	111.1	114.1	116.6
∠O−O−H	101.6	99.7	–	–	–	–	–	–

[a] Bond lengths are in Angstroms and bond angles are in degrees.

TABLE 3: B3LYP/6-311++G(d,p) Harmonic Frequencies (cm^{-1}) of the Peroxyformate Anion and Peroxyformyl Radical

		peroxyformate anion ($\tilde{X}^1A'$)		peroxyformyl radical ($\tilde{X}^2A''$)		peroxyformyl radical ($\tilde{A}^2A'$)	
ν	symmetry	*cis*	*trans*	*cis*	*trans*[a]	*cis*	*trans*
1	A′	2851	2952	3070	3053	3081	3080
2		1724	1690	1878	1889 (1821.5[b])	1837	1851
3		1396	1335	1362	1335	1371	1379
4		1203	1286	1102	1146 (1078[c])	1005	1016
5		834	866	865	954 (957.3[b]; 966[c])	900	954
6		748	607	777	586 (574[c])	748	586
7		296	370	244	404	254	333
8	A″	960	1043	975	1009	994	997
9		405	220	323	175	382	195

[a] Experimental values are provided in parentheses. [b] Ar matrix; ref 19. [c] gas-phase: this work.

fundamental ($4_0^1 5_0^1$ and $4_0^1 5_0^2$, respectively), while peak h3 is due to two quanta of ν_4 on the ν_5 fundamental ($4_0^2 5_0^1$). The extended progressions in these two modes enable a more accurate determination of fundamental vibrational frequencies, as well as crude measurements of the anharmonicity of each mode. Using the expression for the energy differences between vibrational levels of an anharmonic oscillator,

$$g(n) - g(0) = \omega\left(n + \frac{1}{2}\right) - \chi\left(n + \frac{1}{2}\right)^2 - \frac{1}{2}\omega + \frac{1}{4}\chi \tag{9}$$

we can estimate the harmonic frequencies (ω) and anharmonicity constants (χ) for these two modes; here, $g(n)$-$g(0)$ is the energy difference between n and 0 quanta of a given mode.

The harmonic frequency and anharmonicity constant for the C−OO stretch (ν_5) were found using the 5_0^n ($n = 0-3$) and $4_0^1 5_0^n$ ($n = 0-2$) progressions to be $\omega_5 = 973 \pm 20$ cm^{-1} and $\chi_5 = 4 \pm 3$ cm^{-1}. The harmonic frequency and anharmonicity term for the O−O stretch (ν_4) were found using the $4_0^n 5_0^1$ ($n = 0-2$) progression to be $\omega_4 = 1098 \pm 20$ cm^{-1} and $\chi_4 = 10 \pm 5$ cm^{-1}. Using these parameters, the ν_5 and ν_4 fundamental frequencies were determined to be 966 ± 20 and 1078 ± 20 cm^{-1}, respectively. The intense, broad series of peaks primarily derives its intensity from an extended progression in the ν_5 C−OO stretch (5_0^n), along with two combination band progressions ($4_0^1 5_0^n$ and $4_0^2 5_0^n$). At larger binding energies, higher order combination bands ($4_0^m 5_0^n$) congest the spectrum. The low intensity peak d is the fundamental of the ν_6 OCO bend at 574 ± 35 cm^{-1}, while peaks f and h are due to combination bands of one quanta of the ν_6 OCO bend on the ν_5 progression ($5_0^n 6_0^1$, where $n = 1, 2$). Peaks a and c are due to excited anion vibrations. Peak a is the fundamental of the anion ν_6 OCO bend at 587 ± 30 cm^{-1}, while peak c is a sequence band of one quanta of the anion ν_6 OCO bend with the radical ν_5 C−OO stretch ($5_0^1 6_1^0$). Since we were unable to change the anion temperature, the assignment of these anion hot bands is based solely on the spectral simulation.

Following the analysis of the $\tilde{X}^2A''$ state vibronic features, it appears that the discrepancy between the simulated and the experimental spectrum largely stems from the overestimate of the O−O stretching frequency (see Table 3). In actuality, the frequencies of O−O and C−OO stretches are closer to one another than predicted and, therefore, these two modes are only partially resolvable. Additionally, at higher binding energies anharmonic effects are manifested and the harmonic simulation overestimates the peak positions. Using the experimentally determined electron binding energy, frequencies, and anharmonicity constants in the Franck−Condon simulation (Figure 2c) greatly improves its quality; this improvement gives considerable confidence that all of the major features in the *trans*-peroxyformate anion shown in Figure 1a can be assigned to vibrational levels of the ground state of the radical.

The sole exception to this claim is the narrow peak l at 3.27 eV eBE, which is notably absent in the simulation in Figure 1b. The narrowness of this peak (as well as the location mentioned above) strongly suggest that it does not arise from transitions to the $\tilde{X}^2A''$ ground state of the peroxyformyl radical. Moreover, the photoelectron angular distribution associated with this peak does not fit smoothly into the progression seen for the other ground state vibrational peaks, but is less strongly peaked perpendicular to the laser electric field. Inconsistencies such as these are often an indication that another electronic state is appearing in the spectrum. Indeed, the position of peak l is consistent with a vibronic transition to the $\tilde{A}^2A'$ excited state

in the peroxyformyl radical. The G3MP2B3 calculations locate this state 0.79 eV above the ground state. This electronic state of the radical corresponds to removal of an electron from the in-plane p-orbital on the terminal peroxy oxygen atom of the anion. While only a small portion of this excited state profile is observed, the relative intensities predicted by Franck−Condon simulations for the transition from the $\tilde{X}^1A'$ state of the anion to the $\tilde{A}^2A'$ state of the radical (provided in the Supporting Information) indicate that this peak is either the electronic band origin or the fundamental of the COO bend (ν_7), which has a calculated frequency of 333 cm^{-1} (41 meV). The latter appears more likely. Thus, we report that the $\tilde{A}^2A'$ state of the *trans*-peroxyformyl radical lies $0.783^{+0.060}_{-0.020}$ eV above the ground state; the asymmetric error bar accounts for the possibility that peak l might correspond to the origin of the $\tilde{A}^2A'$ state rather than to one quantum of the COO bend.

Gas-Phase Acidity Measurements. The gas-phase acidity of peroxyformic acid was determined through ion−molecule bracketing experiments. This method is employed when proton transfer equilibrium constant measurements are not feasible; in this case, the neutral peroxyformic acid reagent is not available in pure form. In the ion−molecule bracketing technique, the peroxyformate anion is allowed to react with a series of reference acids and the occurrence or nonoccurrence of proton transfer sets a lower or upper bound on the unknown acidity, respectively. For these bracketing experiments, the peroxyformate anion is formed using the same reaction scheme as in the above photodetachment studies.

The gas-phase acidity of peroxyformic acid was bracketed against five reference acids: formic acid (338.6 ± 0.5 kcal mol^{-1}), acetic acid (341.2 ± 0.5 kcal mol^{-1}), hydrogen sulfide (344.89 ± 0.02 kcal mol^{-1}), *tert*-butylthiol (346.7 ± 0.5 kcal mol^{-1}), and isopropylthiol (347.6 ± 0.5 kcal mol^{-1}).[49] For the reactions of peroxyformate anion with *tert*-butylthiol and isopropylthiol, proton transfer does not occur; instead these reactions proceed exclusively by neutral O atom loss to form the formate anion. Proton transfer was the only pathway observed in the reactions of peroxyformate anion with formic acid and acetic acid. For the reaction with formic acid, proton transfer was confirmed by evaluating the reaction with formic acid-d_1, DCO_2H. In this case, an observed increase in m/z 46 is due to proton transfer, whereas the absence of m/z 45 indicates that neutral O atom loss from the peroxyformate anion does not occur. The reaction with hydrogen sulfide primarily proceeds by O atom loss to form the formate ion. Only a minor amount of the proton transfer product, HS^-, was observed, suggesting that the proton transfer pathway is slightly endothermic. On the basis of these results, the acidity of peroxyformic acid is found to be $\Delta_aG_{298} = 344.0 \pm 3.3$ kcal mol^{-1}, between that of acetic acid and *tert*-butylthiol, where the error bar spans the uncertainty in the acidities of the upper and lower bound reference acids.

While these acidity measurements are simple in their implementation, the interpretation of these results is complicated by the significant structural differences between the peroxy anion and neutral peroxy acid. The electronic dipole moment of peroxyformic acid has previously been measured using microwave spectroscopy, and this value is consistent with a cis-planar structure, where a strong intramolecular hydrogen bond exists between the peroxy hydrogen atom and the carbonyl oxygen atom.[50] Rotation about the OCOO dihedral angle by 180° gives a higher energy trans-conformation, where the peroxy hydrogen atom points out of the plane of symmetry (shown below).

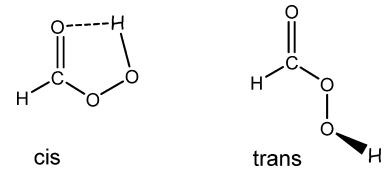

Electronic structure calculations were used to map out the potential energy surface for the trans- to cis-isomerization; these results are summarized in Table 1. For peroxyformic acid, the trans-conformer is 3.4 kcal mol^{-1} higher in energy than the cis-conformer; these two minima are connected by a ∼9.5 kcal mol^{-1} (trans to cis) zero point energy corrected barrier ($\Delta G^{\ddagger} \sim$ 9.8 kcal mol^{-1}). This barrier height is comparable to the free-energy isomerization barrier of methyl formate, which has been determined using dynamic NMR spectroscopy[51] to be 9.85 ± 0.15 kcal mol^{-1}, providing some evidence for the reliability of the calculation. Although these calculations indicate that the isomerization barrier height is less than a typical ion-dipole complexation energy (∼10−20 kcal mol^{-1}),[52] proton transfer is generally barrierless and, therefore, proton transfer rather than isomerization of the anion is expected to occur. As was shown in the above sections, the anion exclusively exists in the trans-conformation. Thus, protonation of the anion initially forms the higher energy trans-conformation of the acid, which then must isomerize to the lower energy cis-conformation. It is, therefore, not immediately clear to which structure the acidity bracket applies.

Whether proton transfer leads to the formation of the cis- or trans-form of the peroxy acid depends on the size of the isomerization barrier and on the overall energetics of the proton transfer reaction. This is qualitatively demonstrated in Figure 4, where the *x*-axis corresponds to the reaction progression for a multidimensional reaction coordinate. For each potential energy surface the total energy of the reaction is given by the dotted line, and the enthalpies of reaction for the trans- and cis-product channels are indicated. As the strength of the reference acid decreases in going from part a to d of Figure 4, the reaction exothermicity decreases; however, the energetics of the two product channels relative to one another remains constant. If proton transfer is sufficiently exothermic (a), then the trans-form of the acid can traverse the isomerization barrier to form the lower energy cis-structure. However, as the strength of the reference acid decreases (b), the reaction complex does not contain sufficient energy and the acid cannot surmount the isomerization barrier. In this scenario, proton transfer exclusively leads to the formation of the trans-form of the acid, even though the cis-product channel is more exothermic. Similarly, as the strength of the reference acid is further decreased such that the formation of the trans-form of the acid is endothermic (c), the reaction does not occur even though the cis-product channel is still exothermic. Of course, the reaction will also not occur if both product channels are endothermic (d).

Since the difference in the acidities of the upper and lower bound reference acids is smaller than the isomerization barrier, the above acidity measurement of $\Delta_aG_{298} = 344.0 \pm 3.3$ kcal mol^{-1} corresponds to the trans-form of the peroxyformate anion going to the trans-form of the peroxyformic acid. Thus, these bracketing experiments probe the gas-phase acidity of the higher energy conformer of the peroxy acid! It should be noted that a similar scenario would exist for the reverse gas-phase acidity bracket, where peroxyformic acid is reacted with a series of reference anions of known basicity. In this case, the peroxy acid is in the cis-conformation.[50,53,54] Proton abstraction would initially result in the formation of the cis-conformer of the anion, which then would have to surmount a significant isomerization

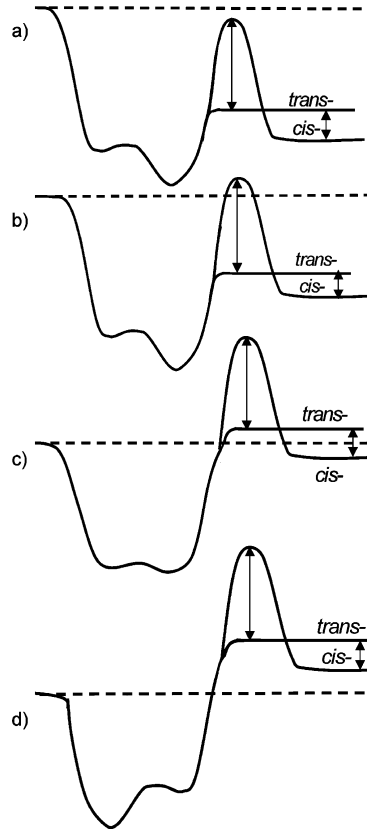

Figure 4. Representative potential energy surfaces for the proton transfer reaction of the trans-conformer of the peroxyformate anion with a reference acid where (a) the reaction is exothermic and both the *trans*- and *cis*-peroxyacids are formed; (b) the reaction is exothermic and only the *trans*-peroxyacid is formed; (c) formation of the *cis*-peroxyacid is exothermic; however, no reaction occurs; and (d) the reaction is endothermic.

barrier (Table 1) to form the lower energy trans-conformer. This acidity bracket would, therefore, probe the gas-phase basicity of the cis-conformer of the peroxy anion. Unfortunately, since we were unable to obtain a pure sample of peroxyformic acid, these experiments were not performed.

Given the complex nature of this peroxy acid system, it seems that the best approach to determine the gas-phase acidity of the lower energy conformer of the *cis*-peroxy acid is to use the calculated energy difference between the two isomers (Table 1). In this case, computations are expected to accurately predict the relative stability, since the systematic errors from the ab initio method are probably similar for both conformers and, therefore, cancel out in the energy difference. On the basis of this approach, the gas-phase acidity of *cis*-peroxyformic acid is determined to be 346.8 ± 3.3 kcal mol^{-1}. Combining our results with the calculated entropy of deprotonation ($\Delta_a S_{298}$) allows for the determination of the enthalpy of deprotonation, $\Delta_a H_{298}$(*cis*-HC(O)OOH) = 354.4 ± 3.3 kcal mol^{-1}; $\Delta_a H_{298}$(*trans*-HC(O)OOH) = 351.1 ± 3.3 kcal mol^{-1},[55] where in both cases deprotonation leads to the trans-form of the anion. It should be noted that peroxyformic acid is slightly more acidic than carbonic acid (HOC(O)OH); in ion−molecule bracketing studies,[48] the bicarbonate ion rapidly proton transfers with *tert*-butylthiol and isopropylthiol, but not with ethanethiol.

Thermochemistry. Accurate knowledge of the peroxy acid O−H bond dissociation energies (BDE, D_0) is important in atmospheric chemistry, low-temperature combustion, and synthetic organic chemistry.[56–58] The OH BDE of peroxyformic acid can be determined from the above electron affinity and enthalpy of deprotonation measurements using a negative ion thermochemical cycle.[21–24]

$$D_o(\mathrm{HC(O)OOH}) = \Delta_a H_o(\mathrm{HC(O)OOH}) + \mathrm{EA(HC(O)OO)} - \mathrm{IE(H)} \quad (10)$$

Here, $\Delta_a H_o$(HC(O)OOH) is the OH deprotonation enthalpy of peroxyformic acid at 0 K, EA(HC(O)OO) is the electron affinity of the peroxyformyl radical, and IE(H) is the ionization energy of the hydrogen atom (13.59844 eV).[59] A small thermal correction is applied to convert the 298 K experimental enthalpy of deprotonation to 0 K (eq 11); the integrated heat capacities are found from electronic structure calculations.

$$\Delta_a H_o(\mathrm{HC(O)OOH}) = \Delta_a H_{298}(\mathrm{HC(O)OOH}) - \int_0^{298}[C_p(\mathrm{HC(O)OO^-}) + C_p(\mathrm{H^+}) - C_p(\mathrm{HC(O)OOH})]\,\mathrm{dT} \quad (11)$$

From the data presented here, the BDEs of both the cis- and trans-conformers of peroxyformic acid can be determined. For both cases, the BDE is defined as the reaction forming the lowest energy trans-conformation of the radical, as shown in Figure 5. The D_0(O−H) for the cis-conformer of peroxyformic acid is determined to be 97.1 ± 3.3 kcal mol^{-1}, while the BDE for the trans-conformer is determined to be 94.0 ± 3.3 kcal mol^{-1}. The uncertainty in the BDE measurements mainly reflects the error in the gas-phase acidity measurements. These BDEs along with other thermochemical values reported in this work are summarized in Table 4.

The O−H BDEs of peroxyformic acid are significantly larger than those of hydrogen peroxide[28] and of peroxy alcohols,[26] which range from 84 to 87 kcal mol^{-1}. This greater bond strength can be attributed to two factors: (1) the strong intramolecular hydrogen bond that is formed between the peroxy hydrogen atom and the carbonyl oxygen atom and (2) a reduction in the repulsive interaction between the O−H bonding orbital and lone pair of electrons on the neighboring oxygen atom through electron back-bonding effects. To illustrate the second factor, consider a resonance structure of a peroxy acid where there is a partial positive charge on the neighboring oxygen atom (shown below), which reduces the unfavorable lone-pair−bonding-pair interaction and increases the double bond character of the C−OO bond. Cleavage of the O−H bond not only breaks the hydrogen bond but also elongates the C−OO bond (by ∼0.09 Å; see Table 2), reducing the C−OO double bond character.

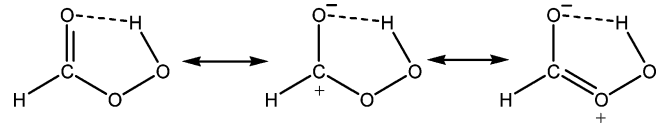

The magnitude of this type of stabilization is approximately equal to the difference in bond strengths of the *trans*-peroxyformic acid, where there is no hydrogen bonding, and of a peroxy alcohol. As in a peroxy alcohol, the lone-pair−bonding-pair repulsion is also minimized in the *trans*-peroxyformic acid since the peroxy hydrogen atom lies out of the ROO plane of symmetry.

The OH BDE of peroxyformic acid lies between that of hydrogen peroxide [$D_0(H_2O_2)$ = 86.6 ± 0.5 kcal mol^{-1}][28] and

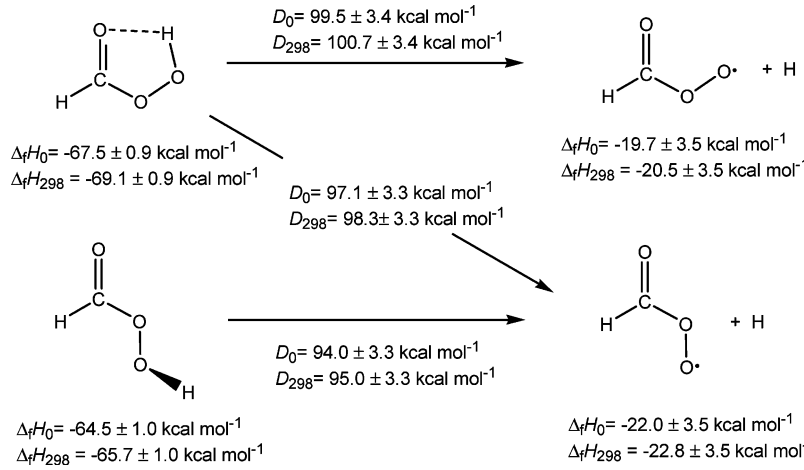

Figure 5. Summary of the bond dissociation energies and heats of formation at 0 and 298 K.[55] The heat of formation of peroxyformic acid is calculated at the G3MP2B3 level of theory (eq 12). The bond dissociation energies are experimentally determined here (eqs 10 and 11); a small energy correction is applied to the bond dissociation energy for *cis*-HC(O)OOH → *trans*-HC(O)OO + H and for *cis*-HC(O)OOH → *cis*-HC(O)OO + H (see the text). The heat of formation of the peroxyformyl radical is determined from the heat of formation of peroxyformic acid and the corresponding bond dissociation energy (eqs 13 and 14).

TABLE 4: Thermochemical Parameters.[a]

peroxyformyl radical and peroxyformic acid	
EA(*trans*-HC(O)OO)	2.493 ± 0.006 eV
T_e $\tilde{A}-\tilde{X}$ (*trans*-HC(O)OO)	$0.783^{+0.060}_{-0.020}$ eV
$\Delta_a G_{298}$(*trans*-HC(O)OO−H)[b]	344.0 ± 3.3 kcal mol^{-1}
$\Delta_a G_{298}$(*cis*-HC(O)OO−H)[c]	346.8 ± 3.3 kcal mol^{-1}
$\Delta_a H_{298}$(*trans*-HC(O)OO−H)[d]	351.1 ± 3.3 kcal mol^{-1}
$\Delta_a H_{298}$(*cis*-HC(O)OO-H)[d]	354.4 ± 3.3 kcal mol^{-1}
D_0(*trans*-HC(O)OO−H)[e]	94.0 ± 3.3 kcal mol^{-1}
D_0(*cis*-HC(O)OO−H)[e]	97.1 ± 3.3 kcal mol^{-1}
$\Delta_f H_{298}$(*trans*-HC(O)OO−H)[f]	−65.7 ± 1.0 kcal mol^{-1}
$\Delta_f H_{298}$(*cis*-HC(O)OO-H)[f]	−69.1 ± 0.9 kcal mol^{-1}
$\Delta_f H_{298}$(*cis*-HC(O)OO)[g]	−20.5 ± 3.5 kcal mol^{-1}
$\Delta_f H_{298}$(*trans*-HC(O)OO)[g]	−22.8 ± 3.5 kcal mol^{-1}

[a] All energy changes correspond to formation of the trans-conformation of the anion or radical, which are the most stable forms. [b] Bracketed between the acidity of acetic acid and *tert*-butylthiol. [c] Determined from the *trans*-peroxyacid acidity and the calculated energy difference between cis- and trans-conformers (see the text). [d] Calculated from the corresponding $\Delta_a G_{298}$ and $\Delta_a S_{298}$. [e] Calculated using the EA, $\Delta_a H_{298}$, IE(H), and a small thermochemical correction [f] Calculated from G3B3MP2 calculations. [g] Determined from the corresponding $\Delta_f H_0$(HC(O)OO−H) and D_0(HC(O)OO−H).

of formic acid [D_0(HC(O)OH) = 112.3 ± 0.8 kcal mol^{-1}].[49,60] Thus, a simple picture that views this OH bond as having character of both hydrogen peroxide and a carboxylic acid appears to be reasonable. On the other hand, the electron binding energy of the peroxyformate anion is much closer to that of formate anion [EA(HC(O)O) = 3.498 ± 0.015 eV][60] than to that of hydrogen peroxide anion [(EA(HO_2) = 1.078 ± 0.006 eV].[28] The greater electron affinity of the peroxyformyl radical is due to the electron-withdrawing effects of the carbonyl group, which stabilizes the corresponding anion. The gas-phase acidity of peroxyformic acid is also closer to that of formic acid [$\Delta_a G_{298}$(HC(O)OH) = 338.6 ± 0.5 kcal mol^{-1}][49] than to that of hydrogen peroxide [$\Delta_a G_{298}$(H_2O_2) = 369.5 ± 0.4 kcal mol^{-1}].[28] In this case, the greater acidity (i.e., lower $\Delta_a G_{298}$) of peroxyformic acid is also due to the stabilization of the corresponding deprotonated anion; however, since the peroxyformic acid is also more stable than hydrogen peroxide, the difference between the acidities of these two types of peroxy compounds is less than the difference in the corresponding electron affinities.

At present, there exists no experimental determination for the heat of formation of peroxyformic acid. Using G3MP2B3 calculations, we have calculated the heat of formation of peroxyformic acid from the following isodesmic reaction:

$$HC(O)OOH + H_2O \rightarrow HC(O)OH + H_2O_2 \quad (12)$$

The heat of formation of the peroxy acid is determined from the calculated heat of reaction and the known heats of formation of the other three compounds.[61] Since the bonding environments in the reactants and products are similar, the systematic errors from the ab initio method cancel, and therefore, this method is expected to produce reasonably good heats of formation for closed shell species. Using this method, the heat of formation at 298 K of *cis*-peroxyformic acid was determined to be −69.1 ± 0.9 kcal mol^{-1}, where the error bar accounts for the uncertainty in the heats of formation of H_2O, H_2O_2, and HC(O)OH, as well as an estimated uncertainty of ±0.5 kcal mol^{-1} in the calculated reaction enthalpy. This value is slightly less than the CCSD(T)/CBS atomization energy calculation of Feller et al.;[62] however, the difference in these two values is approximately equal to the relative stability of the cis- and trans-conformers and, therefore, it is unclear to which conformer Feller's value applies.

The heat of formation of the peroxyformyl radical [$\Delta_f H_{298}$(HC(O)OO)] can be determined from the calculated heats of formation of peroxyformic acid [$\Delta_f H_{298}$(HC(O)OOH)] and the above O−H BDE measurements [D_{298}(HC(O)OO−H)] using eq 13, where the heat of formation of hydrogen atom[59] [$\Delta_f H_{298}$(H)] is 52.103 ± 0.001 kcal mol^{-1}.

$$\Delta_f H_{298}(HC(O)OO) = D_{298}(HC(O)OOH) + \Delta_f H_{298}(HC(O)OOH) - \Delta_f H_{298}(H) \quad (13)$$

Again a small thermal correction, shown in eq 14, is needed to adjust the BDE of HC(O)OO−H from 0 to 298 K

$$D_{298}(\mathrm{HC(O)OO-H}) = D_0(\mathrm{HC(O)OO-H}) + \int_0^{298}[C_p(\mathrm{HC(O)OO}) + C_p(\mathrm{H}) - C_p(\mathrm{HC(O)OOH})]\,\mathrm{dT} \quad (14)$$

The heat of formation of the *trans*-peroxyformyl radical is determined to be -22.8 ± 3.5 kcal mol^{-1}. These values, along with the heats of formation of the higher energy conformers, are summarized in Figure 5.

In an effort to more fully characterize the thermochemistry of acyl peroxy compounds, we have recently performed a similar study on the peroxyacetate anion [$CH_3C(O)OO^-$]. This work will be presented in a forthcoming paper.[32]

Conclusions

The 351.1 nm photoelectron spectrum of the *trans*-peroxyformate anion was measured. On the basis of Franck−Condon simulations, the observed spectral profile is exclusively attributed to the trans-form of the anion. The EA of the *trans*-peroxyformyl radical was determined to be 2.493 ± 0.006 eV and the T_e of the $\tilde{A}^2A'$ state is $0.783^{+0.060}_{-0.020}$ eV. In the $\tilde{X}^2A''$ state of the *trans*-peroxyformyl radical, the harmonic frequency and anharmonicity correction are $\omega_5 = 973 \pm 20$ cm^{-1} and $\chi_5 = 4 \pm 3$ cm^{-1} for the ν_5 C−OO stretch and $\omega_4 = 1098 \pm 20$ cm^{-1} and $\chi_4 = 10 \pm 5$ cm^{-1} for the ν_4 O−O stretch. The fundamental frequency of the in-plane OCO bend is 574 ± 35 cm^{-1}. The gas-phase acidity of *trans*-peroxyformic acid was bracketed between the acidity of acetic acid and *tert*-butylthiol, Δ_aG_{298}(*trans*-peroxyformic acid) $= 344.0 \pm 3.3$ kcal mol^{-1} and Δ_aH_{298}(*trans*-peroxyformic acid) $= 351.1 \pm 3.3$ kcal mol^{-1}. The gas-phase acidity of *cis*-peroxyformic acid was found from the trans-conformer acidity and a calculated energy correction to be Δ_aG_{298}(*cis*-peroxyformic acid) $= 346.8 \pm 3.3$ kcal mol^{-1} and Δ_aH_{298}(*cis*-peroxyformic acid) $= 354.4 \pm 3.3$ kcal mol^{-1}. The OH BDE values for both the cis- and trans-conformers were determined using a negative ion thermodynamic cycle to be D_0(*trans*-peroxyformic acid) $= 94.0 \pm 3.3$ kcal mol^{-1} and D_0(*cis*-peroxyformic acid) $= 97.1 \pm 3.3$ kcal mol^{-1}. Using experimental bond dissociation energy and the G3MP2B3 ab initio electronic structure derived heat of formation for peroxyformic acid, we determine the heats of formation of the *trans*-peroxyformyl radical to be -22.8 ± 3.5 kcal mol^{-1}.

Acknowledgment. We are grateful to Prof. John F. Stanton, Prof. Kent M. Ervin, and Prof. Charles H. DePuy for helpful discussions and suggestions. Additionally, we acknowledge Ms. Kristen M. Volgelhuber for assisting in the photoelectron spectroscopy experiments. This work is supported by the AFOSR (FA9550-09-1-0046). In addition, W.C.L. acknowledges support from NSF (CHE0809391 and PHY0551010), V.M.B. acknowledges NSF (CHE-0647088), and G.B.E. acknowledges support from the DOE (DE-FG02-93ER14364) and from NSF (CHE-0848606). The computational results are based upon work supported by the National Science Foundation under the following NSF programs: Partnerships for Advanced Computational Infrastructure, Distributed Terascale Facility (DTF), and Terascale Extensions: Enhancements to the Extensible Terascale Facility.

Supporting Information Available: The Franck−Condon simulation for transitions from $\tilde{X}^1A'$ state of the *trans*-peroxyformate anion to the $\tilde{A}^2A'$ state of the *trans*-peroxyformyl radical is provided in Figure S1. This material is available free of charge via the Internet at http://pubs.acs.org.

References and Notes

(1) Washida, N.; Martinez, R. I.; Bayes, K. D. Z. *Naturforsch., A: Phys. Sci.* **1974**, *A 29*, 251.
(2) Shibuya, K.; Ebata, T.; Obi, K.; Tanaka, I. *J. Phys. Chem.* **1977**, *81*, 2292.
(3) Clark, J. H.; Moore, C. B.; Reilly, J. P. *Int. J. Chem. Kinet.* **1978**, *10*, 427.
(4) Nadtochenko, V. A.; Sarkisov, O. M.; Vedeneev, V. I. *Dokl. Akad. Nauk Sssr* **1979**, *244*, 152.
(5) Gill, R. J.; Johnson, W. D.; Atkinson, G. H. *Chem. Phys.* **1981**, *58*, 29.
(6) Veyret, B.; Lesclaux, R. *J. Phys. Chem.* **1981**, *85*, 1918.
(7) Langford, A. O.; Moore, C. B. *J. Chem. Phys.* **1984**, *80*, 4211.
(8) Temps, F.; Wagner, H. G. *Ber. Bunsen-Ges. Phys. Chem.* **1984**, *88*, 410.
(9) Timonen, R. S.; Ratajczak, E.; Gutman, D. *J. Phys. Chem.* **1988**, *92*, 651.
(10) Nesbitt, F. L.; Gleason, J. F.; Stief, L. J. *J. Phys. Chem. A* **1999**, *103*, 3038.
(11) Ninomiya, Y.; Goto, M.; Hashimoto, S.; Kagawa, Y.; Yoshizawa, K.; Kawasaki, M.; Wallington, T. J.; Hurley, M. D. *J. Phys. Chem. A* **2000**, *104*, 7556.
(12) Yamasaki, K.; Sato, M.; Itakura, A.; Watanabe, A.; Kakuda, T.; Tokue, I. *J. Phys. Chem. A* **2000**, *104*, 6517.
(13) DeSain, J. D.; Jusinski, L. E.; Ho, A. D.; Taatjes, C. A. *Chem. Phys. Lett.* **2001**, *347*, 79.
(14) Radford, H. E.; Evenson, K. M.; Howard, C. J. *J. Chem. Phys.* **1974**, *60*, 3178.
(15) Hsu, C. C.; Mebel, A. M.; Lin, M. C. *J. Chem. Phys.* **1996**, *105*, 2346.
(16) Winter, N. W.; Goddard, W. A.; Bender, C. F. *Chem. Phys. Lett.* **1975**, *33*, 25.
(17) Tso, T. L.; Diem, M.; Lee, E. K. C. *Chem. Phys. Lett.* **1982**, *91*, 339.
(18) Tso, T. L.; Lee, E. K. C. *J. Phys. Chem.* **1984**, *88*, 5465.
(19) Yang, R. J.; Yu, L. A.; Zeng, A. H.; Zhou, M. F. *J. Phys. Chem. A* **2004**, *108*, 4228.
(20) Yang, H. C.; Chen, H. L.; Ho, J. J. *J. Mol. Struct. Theochem.* **2006**, *774*, 35.
(21) Berkowitz, J.; Ellison, G. B.; Gutman, D. *J. Phys. Chem.* **1994**, *98*, 2744.
(22) Blanksby, S. J.; Ellison, G. B. *Acc. Chem. Res.* **2003**, *36*, 255.
(23) Ervin, K. M.; Gronert, S.; Barlow, S. E.; Gilles, M. K.; Harrison, A. G.; Bierbaum, V. M.; DePuy, C. H.; Lineberger, W. C.; Ellison, G. B. *J. Am. Chem. Soc.* **1990**, *112*, 5750.
(24) Wenthold, P. G.; Lineberger, W. C. *Acc. Chem. Res.* **1999**, *32*, 597.
(25) Clifford, E. P.; Wenthold, P. G.; Gareyev, R.; Lineberger, W. C.; DePuy, C. H.; Bierbaum, V. M.; Ellison, G. B. *J. Chem. Phys.* **1998**, *109*, 10293.
(26) Blanksby, S. J.; Ramond, T. M.; Davico, G. E.; Nimlos, M. R.; Kato, S.; Bierbaum, V. M.; Lineberger, W. C.; Ellison, G. B.; Okumura, M. *J. Am. Chem. Soc.* **2001**, *123*, 9585.
(27) Blanksby, S. J.; Ellison, G. B.; Bierbaum, V. M.; Kato, S. *J. Am. Chem. Soc.* **2002**, *124*, 3196.
(28) Ramond, T. M.; Blanksby, S. J.; Kato, S.; Bierbaum, V. M.; Davico, G. E.; Schwartz, R. L.; Lineberger, W. C.; Ellison, G. B. *J. Phys. Chem. A* **2002**, *106*, 9641.
(29) Blanksby, S. J.; Kato, S.; Bierbaum, V. M.; Ellison, G. B. *Aust. J. Chem.* **2003**, *56*, 459.
(30) Blanksby, S. J.; Bierbaum, V. M.; Ellison, G. B.; Kato, S. *Angew. Chem.* **2007**, *46*, 4948.
(31) Kato, S.; Ellison, G. B.; Bierbaum, V. M.; Blanksby, S. J. *J. Phys. Chem. A* **2008**, *112*, 9516.
(32) Villano, S. M.; Eyet, N.; Wren, S. W.; Ellison, G. B.; Bierbaum, V. M.; Lineberger, W. C. *Eur. J. Mass Spectrom.* **2009**, submitted.
(33) Ervin, K. M.; Lineberger, W. C. Photoelectron Spectroscopy of Negative Ions. In *Advances in Gas Phase Ion Chemistry*; Adams, N. G., Babcock, L. M., Eds.; JAI Press: Greenwich, 1992; Vol. 1; pp 121.
(34) Ramond, T. M.; Davico, G. E.; Schwartz, R. L.; Lineberger, W. C. *J. Chem. Phys.* **2000**, *112*, 1158.
(35) DePuy, C. H.; Della, E. W.; Filley, J.; Grabowski, J. J.; Bierbaum, V. M. *J. Am. Chem. Soc.* **1983**, *105*, 2481.
(36) Bowie, J. H.; DePuy, C. H.; Sullivan, S. A.; Bierbaum, V. M. *Can. J. Chem.-Rev. Can. Chim.* **1986**, *64*, 1046.
(37) Hotop, H.; Lineberger, W. C. *J. Phys. Chem. Ref. Data* **1985**, *14*, 731.
(38) Cooper, J.; Zare, R. N. *J. Chem. Phys.* **1968**, *48*, 942.
(39) Ervin, K. M.; Ramond, T. M.; Davico, G. E.; Schwartz, R. L.; Casey, S. M.; Lineberger, W. C. *J. Phys. Chem. A* **2001**, *105*, 10822.
(40) Van Doren, J. M.; Barlow, S. E.; DePuy, C. H.; Bierbaum, V. M. *Int. J. Mass Spectrom. Ion Processes* **1987**, *81*, 85.

(41) Frisch, M. J. Trucks, G. W.; Schlegel, H. B.; Scuseria, G. E.; Robb, M. A.; Cheeseman, J. R.; Montgomery, J. A.; Vreven, T.; Kudin, K. N.; Burant, J. C.; Millam, J. M.; Iyengar, S. S.; Tomasi, J.; Barone, V.; Mennucci, B.; Cossi, M.; Scalmani, G.; Rega, N.; Petersson, G. A.; Nakatsuji, H.; Hada, M.; Ehara, M.; Toyota, K.; Fukuda, R.; Hasegawa, J.; Ishida, M.; Nakajima, T.; Honda, Y.; Kitao, O.; Nakai, H.; Klene, M.; Li, X.; Knox, J. E.; Hratchian, H. P.; Cross, J. B.; Adamo, C.; Jaramillo, J.; Gomperts, R.; Stratmann, R. E.; Yazyev, O.; Austin, A. J.; Cammi, R.; Pomelli, C.; Ochterski, J. W.; Ayala, P. Y.; Morokuma, K.; Voth, G. A.; Salvador, P.; Dannenberg, J. J.; Zakrzewski, V. G.; Dapprich, S.; Daniels, A. D.; Strain, M. C.; Farkas, O.; Malick, D. K.; Rabuck, A. D.; Raghavachari, K.; Foresman, J. B.; Ortiz, J. V.; Cui, Q.; Baboul, A. G.; Clifford, S.; Cioslowski, J.; Stefanov, B. B.; Liu, G.; Liashenko, A.; Piskorz, P.; Komaromi, I.; Martin, R. L.; Fox, D. J.; Keith, T. Al-Laham, M. A.; Peng; C. Y., Nanayakkara, A.; Challacombe, M.; Gill, P. M. W.; Johnson, B.; Chen, W.; Wong, M. W.; Gonzalez, C.; Pople, J. A. *Gaussian 03*, revision B.05; Gaussian Corp.: Pittsburgh, PA, 2003.

(42) Becke, A. D. *J. Chem. Phys.* **1993**, *98*, 5648.

(43) Krishnan, R.; Binkley, J. S.; Seeger, R.; Pople, J. A. *J. Chem. Phys.* **1980**, *72*, 650.

(44) Lee, C. T.; Yang, W. T.; Parr, R. G. *Phys. Rev. B* **1988**, *37*, 785.

(45) Baboul, A. G.; Curtiss, L. A.; Redfern, P. C.; Raghavachari, K. *J. Chem. Phys.* **1999**, *110*, 7650.

(46) G3MP2B3-calculated values. EA: HO_2 1.061 eV; CH_3OO 1.168 eV; C_2H_5OO 1.175 eV; HC(O)O 3.575 eV; $CH_3C(O)O$ 3.296 eV. $\Delta_a H_0$: H_2O_2 377.1 kcal mol^{-1}; CH_3OOH 373.2 kcal mol^{-1}; C_2H_5OOH 372.8 kcal mol^{-1}; HC(O)OH 342.8 kcal mol^{-1}; $CH_3C(O)OH$ 348.0 kcal mol^{-1}. D_0: H_2O_2 88.0 kcal mol^{-1}; CH_3OOH 86.6 kcal mol^{-1}; C_2H_5OOH 86.4 kcal mol^{-1}; HC(O)OH 113.1 kcal mol^{-1}; $CH_3C(O)OH$ 110.4 kcal mol^{-1}.

(47) Ervin, K. M. *PESCAL*; University of Nevada: Reno, 2003.

(48) Squires, R. R. *Int. J. Mass Spectrom. Ion Processes* **1992**, *117*, 565.

(49) Eyet, N.; Villano, S. M.; Bierbaum, V. M. *Int. J. Mass Spectrom.* **2009**, *283*, 26.

(50) Oldani, M.; Ha, T. K.; Bauder, A. *J. Am. Chem. Soc.* **1983**, *105*, 360.

(51) Cain, D.; Pawar, D. M.; Stewart, M.; Billings, H.; Noe, E. A. *J. Org. Chem.* **2001**, *66*, 6092.

(52) DePuy, C. H. *J. Org. Chem.* **2002**, *67*, 2393.

(53) Cugley, J. A.; Bossert, W.; Bauder, A.; Gunthard, H. H. *Chem. Phys.* **1976**, *16*, 229.

(54) Langley, C. H.; Noe, E. A. *J. Mol. Struct. Theochem.* **2004**, *682*, 215.

(55) The 0.1 kcal mol^{-1} discrepancy with Table 1 is due to rounding.

(56) Kirchner, F.; Stockwell, W. R. *J. Geophys. Res. Atmos.* **1996**, *101*, 21007.

(57) Lightfoot, P. D.; Cox, R. A.; Crowley, J. N.; Destriau, M.; Hayman, G. D.; Jenkin, M. E.; Moortgat, G. K.; Zabel, F. *Atmos. Environ. Part A* **1992**, *26*, 1805.

(58) Madronich, S.; Greenberg, J.; Paulson, S.; Orlando, J. J.; Tyndall, G. S. Organic Compounds. In *Atmospheric Chemistry and Global Change*; Brasseur, G. P., Orlando, J. J., Tyndall, G. S., Eds.; Oxford University Press: Oxford, 1999; pp 325.

(59) *NIST Chemistry WebBook, NIST Standard Reference Database Number 69*; Linstrom, P. J., Mallard, W. G., Eds.; National Institute of Standards and Technology: Gaithersburg, MD, 2005.

(60) Kim, E. H.; Bradforth, S. E.; Arnold, D. W.; Metz, R. B.; Neumark, D. M. *J. Chem. Phys.* **1995**, *103*, 7801.

(61) $\Delta_f H_{298}(H_2O) = -57.7978 \pm 0.0096$ kcal mol^{-1} [Cox, J. D.; Wagman, D. D.; Medvedev, V. A. *CODATA Key Values for Thermodynamics*; Hemisphere Publishing Corp.: New York, 1984; p 1]; $\Delta_f H_{298}(H_2O_2) = -32.48 \pm 0.05$ kcal mol^{-1} [*Thermodynamic Properties of Individual Substances,* 4th ed.;Gurvich, L. V., Veyts, I. V., Alcock, C. B., Eds.; Hemisphere: New York, 1989; Vol. 1]; $\Delta_f H_{298}(HCO_2H) = -90.52 \pm 0.73$ kcal mol^{-1} [average of five values:Gunthrie, J. P. *J. Am. Chem. Soc.* **1974**, *96*, 3608. Lebedeva, N. D. *Russ. J. Phys. Chem.* **1964**, *38*, 1435. Sinke, G. C. *J. Phys. Chem.* **1959**, *63*, 2063].

(62) Feller, D.; Dixon, D. A.; Francisco, J. S. *J. Phys. Chem. A* **2003**, *107*, 1604.

JP907569W